Pergamon

Int. J. Heat Mass Transfer. Vol. 41, No. 11, pp. 1601–1611, 1998

Printed in Great Britain
0017–9310/98 $19.00+0.00

PII: S0017–9310(97)00271–8

Oscillatory double-diffusive convection in a rectangular enclosure with combined horizontal temperature and concentration gradients

TATSUO NISHIMURA,* MIKIO WAKAMATSU and ALEXANDRU M. MOREGA

Department of Mechanical Engineering, Yamaguchi University, Ube 755, Japan

(*Received* 20 *December* 1996)

Abstract—The effect of buoyancy ratio on the flow structure is investigated numerically for a binary mixture gas in a rectangular enclosure subject to opposing horizontal thermal and compositional buoyancies. The following conditions were considered: $Ra_T = 10^5$, $Pr = 1$, $Le = 2$ and $N = 0.0$–2.0 for $A = 2$. The numerical solution predicts that oscillatory double-diffusive convection with the secondary cell flow structure occurs for a certain range of buoyancy ratio. The key mechanism for oscillatory flow is that the unstably stratified region of species shifts from the central part of the enclosure to the upper and lower parts, and vice versa in a time-periodic sense, due to the interaction of heat and mass transfer with different diffusivities near the vertical walls. Bifurcation structures of the oscillatory flow in the present system are discussed.

INTRODUCTION

Natural convection due to spatial variations of fluid density is of fundamental importance in many natural and industrial problems. Recently, there has been increased interest in the role that double-diffusive natural convection plays in physical and chemical vapor transport processes [1–3] and crystal-growth techniques such as semi-conductors and alloys [4–8].

In a number of the experimental and numerical studies, it has been found that oscillatory flow is caused by the interaction between thermal and compositional processes under a certain range of buoyancy ratio. The buoyancy ratio is defined as the ratio of compositional buoyancy force to thermal buoyancy force. Kamotani *et al.* [9] and Jiang *et al.* [10] investigated experimentally natural convection in shallow enclosures filled with electrolytic solutions for high Lewis numbers, due to combined horizontal thermal and solutal gradients. For different buoyancy ratios, multilayer, secondary cell and mixed flow structures were observed. Significant fluctuations in velocity, temperature and concentration can be observed in the secondary cell flow. Chang and Lin [11] examined numerically thermo-solutal opposing convection in a salt-water solution at high thermal Rayleigh numbers and found that the flow follows a quasi-periodic route to chaos under certain conditions. Bergman and Hyun [12] studied numerically double-diffusive convection in liquid metals with low Prandtl numbers, and their predictions at relatively large Rayleigh number and buoyancy ratio indicates a highly oscillatory behavior. Weaver and Viskanta [13] also examined experimentally natural convection in binary gases with low Lewis number for both aiding and opposing flows and showed that the flow is unsteady for opposing case, which was not predicted numerically.

Tsitverblit [14] studied numerically natural convection concerning the lateral heating of a vertical rectangular enclosure containing a stably stratified salt solution and indicated that certain intervals of the buoyancy ratio posses multiple steady flows at high solutal Rayleigh numbers. In a similar system, Kamakura and Ozoe [15] predicted numerically double periodic oscillation at high thermal Rayleigh number.

Although oscillatory flows are observed in several systems, their mechanism has been poorly understood. The present study examined numerically the detailed characteristics of the oscillatory double-diffusive convection in a rectangular enclosure filled with a binary mixture gas for Prandtl and Schmidt numbers of the order of unity, submitted to constant temperature and concentration differences imposed across the vertical walls. The analysis deals with the particular situation where the thermal and compositional buoyancy forces are opposite. Steady flows have been presented for binary mixture gases [16, 17], but oscillatory flows have not been predicted numerically as mentioned above, and the oscillatory characteristics have been unknown. Computations with the unsteady Galerkin finite element method were carried out for the Prandtl number $Pr = 1$, the Lewis number $Le = 2$, the aspect ratio $A = 2$, the thermal Rayleigh number $Ra_T = 10^5$

* Correspondence to: Prof. T. Nishimura, Yamaguchi University, Department of Mechanical Engineering, Ube 755, Japan.

NOMENCLATURE

A	enclosure aspect ratio $= H/W$
c	species concentration
c_l	low concentration
c_h	high concentration
C	dimensionless concentration $=(c-c_l)/(c_h-c_l)-0.5$
D	species diffusivity
g	gravitational acceleration
h	heat transfer coefficient
H	enclosure height
k	mass transfer coefficient
Le	Lewis number $= \alpha/D$
N	buoyancy ratio $= \beta_c(c_h-c_l)/\beta_T(T_h-T_c)$
Nu	overall Nusselt number $= hW/\lambda$
Pr	Prandtl number $= \nu/\alpha$
Ra_T	thermal Rayleigh number $= g\beta_T(T_h-T_c)W^3/\alpha\nu$
Sh	overall Sherwood number $= kW/D$
t	time
t_0	period of oscillation
T	temperature
T_c	cold wall temperature
T_h	hot wall temperature
u	horizontal velocity
U	dimensionless horizontal velocity $= uW/\alpha$
v	vertical velocity
V	dimensionless vertical velocity $= vW/\alpha$
W	enclosure width
x	horizontal coordinate
X	dimensionless horizontal coordinate $= x/W$
y	vertical coordinate
Y	dimensionless vertical coordinate $= y/W$.

Greek symbols

α	thermal diffusivity
β_c	compositional expansion coefficient
β_T	thermal expansion coefficient
δ_c	thickness of compositional boundary layer
ζ	dimensionless vorticity
θ	dimensionless temperature $=(T-T_c)/(T_h-T_c)-0.5$
λ	thermal conductivity
ν	kinematic viscosity
ρ^*	dimensionless density $= N\times C-\theta$
τ	dimensionless time $= \alpha t/W^2$
τ_0	dimensionless period of oscillation $= \alpha t_0/W^2$
ϕ	phase difference between maximum values in thermal and compositional recirculations
Ψ	dimensionless streamfunction
$\lvert\Psi\rvert_{max}$	strength of thermal recirculation
$\lvert\Psi\rvert_{min}$	strength of compositional recirculation.

and different buoyancy ratios in the range $N = 0.0$–2.0, and we presented bifurcation structures of oscillatory flow as a function of buoyancy ratio.

MATHEMATICAL MODEL AND NUMERICAL SOLUTION

The physical system consists of a rectangular enclosure as shown in Fig. 1. Uniform temperature and concentration differences are imposed across the vertical walls, where the thermal buoyancy force retards the compositional buoyancy force, i.e., opposing flow. The top and bottom of the enclosure are considered to be adiabatic and impermeable to mass transfer. The fluid in the enclosure is a binary mixture gas consisting of a phase changeable component and an inert component. One of the vertical surfaces of the enclosure is the source, where the material (phase changeable component) diffuses from the surface towards the bulk fluid of binary mixture. The other vertical surface is the sink, where the material diffuses from the bulk fluid towards the surface. Mathematical models for this system has been given in the literature, e.g., crystal growth by physical vapor deposition [2] and transport of water vapor and air [16]. There have been many factors on the boundary conditions to be considered, e.g., interfacial velocities at the vertical surfaces corresponding to the interfaces of two phases, depending on the concentration difference between the vertical surfaces and the concentration gradient at respective surface and thus double-diffusive convection of binary mixture gas systems is very com-

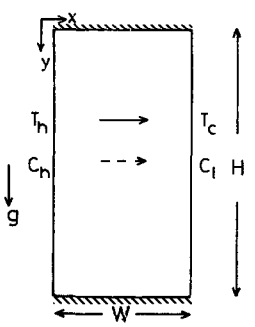

Fig. 1. Physical model.

plicated. In the present study, the following assumptions are given, because we initially understand the fundamental nature of oscillatory double-diffusive convection, apart from the practical concerns.

We consider a system with a small concentration difference between the vertical surfaces because the interfacial velocities have negligible influence on the transport processes according to Ramganathan and Viskanta [18]. The fluid is considered incompressible and Newtonian in behavior with negligible viscous dissipation. Thermophysical properties are assumed to be independent, and also the Boussinesq approximation is utilized. Soret and Dufour effects are neglected, like the other studies.

The governing equations that describe double-diffusive convection are expressed in terms of stream-function, vorticity, temperature and concentration, in dimensionless form as follows:

$$\zeta = \frac{\partial V}{\partial X} - \frac{\partial U}{\partial Y} = -\nabla^2 \Psi \tag{1}$$

$$\frac{\partial \zeta}{\partial \tau} + U\frac{\partial \zeta}{\partial X} + V\frac{\partial \zeta}{\partial Y} = Ra_T Pr\left(-\frac{\partial \theta}{\partial X} + N\frac{\partial C}{\partial X}\right) + Pr\nabla^2 \zeta \tag{2}$$

$$\frac{\partial \theta}{\partial \tau} + U\frac{\partial \theta}{\partial X} + V\frac{\partial \theta}{\partial Y} = \nabla^2 \theta \tag{3}$$

$$\frac{\partial C}{\partial \tau} + U\frac{\partial C}{\partial X} + V\frac{\partial C}{\partial Y} = \nabla^2 C/Le \tag{4}$$

Dimensionless parameters Pr, Ra_T, Le and N are given as follows:

$$Pr = \nu/\alpha \quad Ra_T = g\beta_T(T_h - T_c)W^3/\nu\alpha$$
$$Le = \alpha/D \quad N = \beta_c(C_h - C_l)/\beta_T(T_h - T_c) \tag{5}$$

The boundary conditions that solve the stated problem are

At $Y = 0$ (horizontal top wall)

$$U = V = \Psi = 0, \quad \zeta = -\frac{\partial^2 \Psi}{\partial Y^2}, \quad \frac{\partial \theta}{\partial Y} = 0, \quad \frac{\partial C}{\partial Y} = 0$$

At $Y = H/W$ (horizontal bottom wall)

$$U = V = \Psi = 0, \quad \zeta = -\frac{\partial^2 \Psi}{\partial Y^2}, \quad \frac{\partial \theta}{\partial Y} = 0, \quad \frac{\partial C}{\partial Y} = 0$$

At $X = 0$ (vertical left wall)

$$U = V = \Psi = 0, \quad \zeta = -\frac{\partial^2 \Psi}{\partial X^2}, \quad \theta = 0.5, \quad C = 0.5$$

At $X = 1$ (vertical right wall)

$$U = V = \Psi = 0, \ \zeta = -\frac{\partial^2 \Psi}{\partial X^2}, \ \theta = -0.5, \ C = -0.5$$

Computations were performed using the Galerkin finite element method which is familiar to numerical analysis [19]. The characteristics of the algorithm used here are summarized as follows: (1) Linear triangular elements are used for spatial discretization. (2) The Crank–Nicolson scheme is used for discretization of the time derivative terms, but convective terms are treated explicitly in time and while other terms remain implicit. This finite element method has predicted well self-sustained oscillatory flow in grooved channels for forced convection [20] and also has been employed for several unsteady heat and fluid flow problems, e.g., Kamakura and Ozoe [15].

The accuracy of the numerical scheme has been established by comparison with reference solutions concerning the classical thermal convection problem of air in a rectangular enclosure. For $A = 2$, 21×31 and 31×41 uniform grid systems were used. Overall Nusselt number of the present solution agrees well within 2% discrepancy with other solutions reported by several investigators.

In the present study, the buoyancy ratio is varied for the rectangular enclosure of $A = 2$ while other parameters are held constant ($Pr = 1$, $Ra_T = 10^5$ and $Le = 2$). The selection of $Pr = 1$ and $Le = 2$ was due to the consideration of gas system. The Rayleigh number of 10^5 belongs to the convection regime at $N = 1$, according to the analysis of Gobin and Bennacer [21]. At $N = 1$, the fluid motion occurs above a critical Rayleigh number in this system when the Lewis number is not unity and the predicted critical value in the present numerical scheme agreed well with the result of Gobin and Bennacer under the conditions of $A = 1$, $Pr = 1$ and $Le = 2$.

In particular, we consider two courses of increasing and decreasing buoyancy ratio to examine nonlinear effects in this system, since the previous numerical studies for water–salt solutions [11, 22] provided only fragmentary information on the buoyancy ratio effect under the horizontal temperature and concentration gradients. In the course of increasing buoyancy ratio, we first obtained the steady solution at $N = 0.0$. This solution was employed as the initial guess for solution of the subsequent case of buoyancy ratio, say $N = 0.1$. The latter solution was then used to initiate the computation of the next solution. However, in the transitional flow regime, a smaller increment of $\Delta N = 0.001$ was employed to determine some critical values of buoyancy ratio within 0.001 accuracy. In the course of decreasing buoyancy ratio, we started from the steady solution at $N = 2.0$. Then the similar procedure proceeded continuously, backwards, down to $N = 0.0$.

The predictions reported here have required approximately 8 months of CPU time on Sony News workstation (NWS-50000). The selection of $A = 2$ was motivated by the preliminary computations that were performed for three different aspect ratios $A = 0.5$, 1, 2, and where we found that oscillatory flow occurs only for $A = 2$ under $Pr = 1$, $Ra_T = 10^5$ and $Le = 2$. The results for $A = 0.5$ and 1 have been described in the references [23, 24]. Also the accuracy

test for this problem was performed by comparison of finite element and spectral solutions as shown in the Appendix, and the computation was carried out on 31×41 nodal points. Time steps of the order of 10^{-5} were used.

RESULTS AND DISCUSSION

Steady flow

The vorticity transport eqn (2) suggests that for $N < 1$, the flow is primarily dominated by the thermal buoyancy force and for $N > 1$, the compositional buoyancy force rather than the thermal buoyancy force dominates the flow. In the present case, the interaction between thermal and compositional buoyancy forces is found to be small, except for the buoyancy ratio near unity where the fluid motion is maintained at a steady state.

Figure 2 shows the results for $N = 0.8$ and 1.3 for reference. At $N = 0.8$, the flow is dominated by the thermal buoyancy force, indicating a large clockwise-rotating recirculation (the so-called thermal recirculation). Unlike pure thermal convection, the isotherms are not horizontally uniform in the core region far from the vertical walls, which is affected by the vertical velocity profile. The concentration contours are furthermore distorted in the core. This is due to the species diffusivity being half the thermal diffusivity. The density contours indicate a stable stratification in the vertical direction except near the top and bottom walls. The density is given by $\rho^* = N \times C - \theta$, where the solid and dotted lines denote negative and positive values, respectively. It should be noted that density and temperature profiles are not horizontally uniform in the core region.

At $N = 1.3$, the flow is dominated by the compositional buoyancy force, indicating a counter clockwise-rotating recirculation in the core (the co-called compositional recirculation), although a pair of thermal recirculations exists near the corners of the enclosure. The temperature and concentration contours are parallel to each other within the core, and thus the

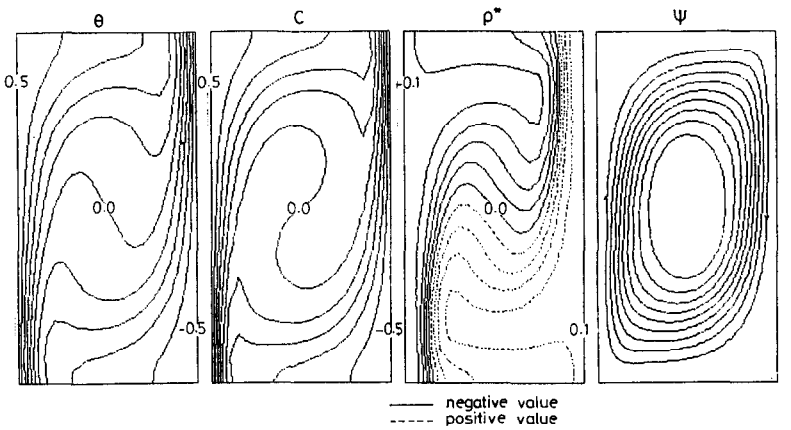

Fig. 2. Steady solutions at $N = 0.8$ and 1.3.

density is horizontally uniform and stably stratified in the vertical direction, different from the results for thermal-dominated flow. These profiles are similar to those for $A = 0.5$ and 1.0 [23, 24].

Oscillatory flow

We found that periodic oscillatory flow appears in a certain range of buoyancy ratio. Figure 3 shows time profiles of the strength of thermal recirculation for several buoyancy ratios in the course of increasing buoyancy ratio. A measure of the recirculation strength is given as the absolute maximum value of the streamfunction of thermal recirculation. The oscillations are periodic and the period is about 0.05, regardless of buoyancy ratio.

Figure 4 shows representative time profiles of the strength of thermal and compositional recirculations at $N = 1$, where the global thermal buoyancy force equals the compositional buoyancy force. The maximum value of thermal recirculation is about five times the compositional recirculation, and there is about 1/4 period delay between the maximum recirculation values. For other buoyancy ratios, similar behaviors are observed. Figure 5 shows the temperature, concentration and streamline contours at four moments during a period of oscillation shown in Fig. 4. At time moment (a), the thermal recirculation reaches its minimum. Two regions of unstable and stable species stratification are located in the central part and in the upper and lower regions of the enclosure, respectively. At the time moment (b), the compositional recirculation attains its minimum. The unstable species stratification in the central part tends to diminish with the growth of the thermal recirculation. At time moment (c), the thermal recirculation is at its maximum and the region of stable species stratification dominates the central part, contrasting with case (a). At time moment (d), when the compositional recirculation reaches its maximum, the stable species stratification in the central part is seen to diminish with a decrease in the thermal recirculation. After a period of oscillation, the thermal and compositional recirculations have the same values as those before a period of oscillation, to complete the cycle.

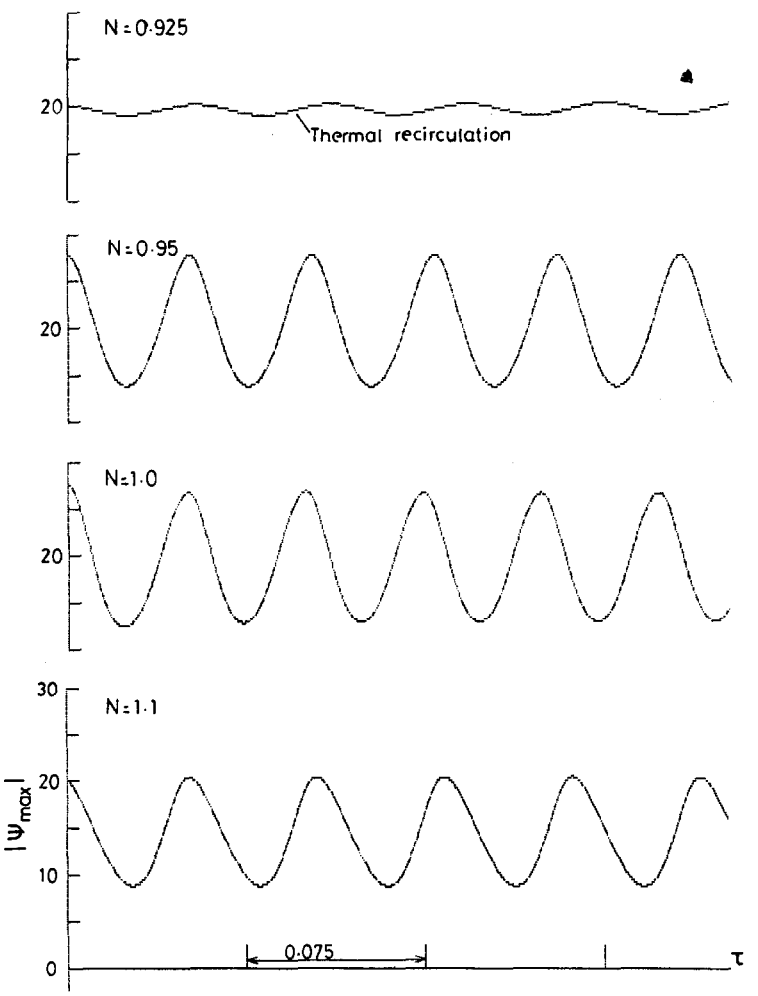

Fig. 3. Time profiles of thermal recirculation for different buoyancy ratios.

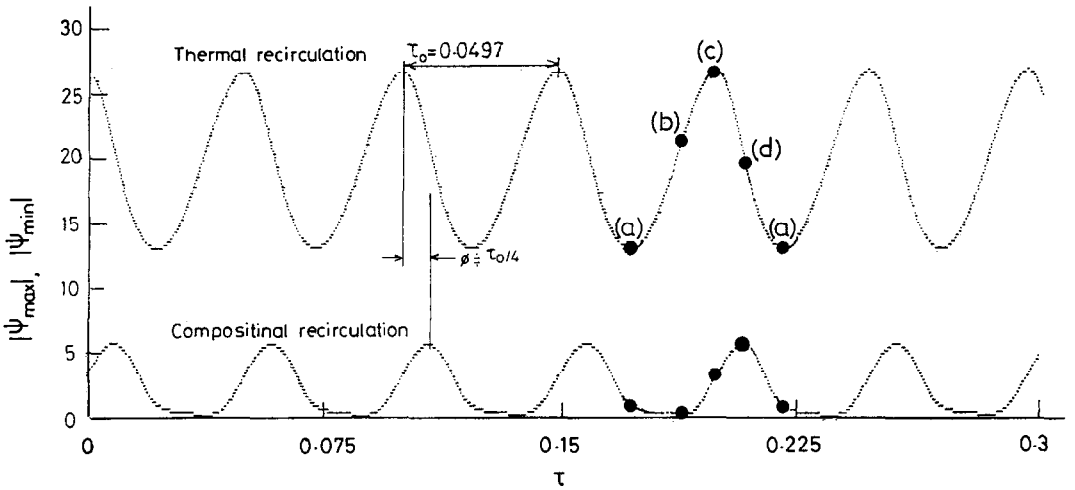

Fig. 4. Time profiles of thermal and compositional recirculations at $N = 1.0$.

Thus the global oscillatory flow evidences a periodic exchange between stable and unstable states in species stratification, due to the interaction between thermal and compositional recirculations. In the central part of the enclosure, increasing and decreasing thermal recirculation leads to this exchange, while the compositional recirculation plays an important role in the exchange at the upper and lower parts.

We discuss next the mechanism of oscillatory flow. To assist our understanding on the oscillatory motion in this system, the previous studies on double-diffusive convection for aqueous solutions with high Lewis and Prandtl numbers are briefly reviewed. Depending on the buoyancy ratio, multilayer, secondary cell and mixed flow structures were identified experimentally and numerically [10, 11]. In particular, the numerical study by Chang and Lin [11] predicted that three flow regimes experience different amplitudes and frequencies for oscillatory flow at a high thermal Rayleigh number. It was suggested that the oscillatory flows result from the complex interactions between the wall boundary layer instability, internal wave instability and thermosolutal instability. On the other hand, in the present study, there are several features different from the results for liquid systems mentioned above. The oscillatory flow keeps only the secondary cell flow structure and the period of oscillation or the frequency is almost constant, regardless of buoyancy ratio. These differences may be primarily due to small thermal Rayleigh and Lewis numbers. It is expected that the oscillation mechanism in the present system belongs to one of the three instabilities suggested by Chang and Lin. The wall boundary instability is not likely to occur as suggested by the isotherms and isoconcentration lines in Fig. 5, because of small thermal Rayleigh number and small buoyancy ratio. The prediction of internal wave instability is difficult due to the interaction between heat and mass transfer. If thermal convection is only considered, the internal Froude number is 0.687 in the present system, following Paolucci and Chenoweth [25] and thus the internal wave does not appear. However, it is beyond our current capability to confirm that the cause of oscillation is not the internal wave in the presence of heat and mass transfer. While, focusing on the flow near the vertical walls in Fig. 5, we notice that opposing thermal and compositional buoyancies meet at a neutral balance point at respective wall, i.e., stagnation point, which is one of the characteristics for the secondary cell flow structure [11]. Thus we believe that the thermosolutal instability is more dominant in the present system, rather than other instabilities.

Here we consider the phase difference between time variations in thermal and compositional recirculations shown in Fig. 4. Figure 6 shows the model of oscillatory flow in the present system. Oscillation leads to a periodic exchange between stable and unstable states in species stratification. The hatched zone denotes the region of unstable stratification and the other zone is stable one. It is thought that there are three different processes such as excitation, relaxation and inhibition of thermal recirculation as a result of the thermosolutal instability and that the excitation in thermal recirculation leads to the decrease of compositional recirculation and a stable species stratification in the central part of the enclosure, while the inhibition leads to the increase of compositional recirculation and an unstable one. We assume sinusoidal profiles of thermal and compositional recirculations with a 1/4 period delay as shown in Fig. 6, which is slightly different from the real case shown in Fig. 4.

During a–b in the figure, an unstable species stratification in the central part of the enclosure is reduced, and therefore the thermal recirculation is increased and the compositional recirculation is decreased. During b–c, the system evolutes towards the subsequent decrease of thermal recirculation, and therefore the compositional recirculation is increased whereas the

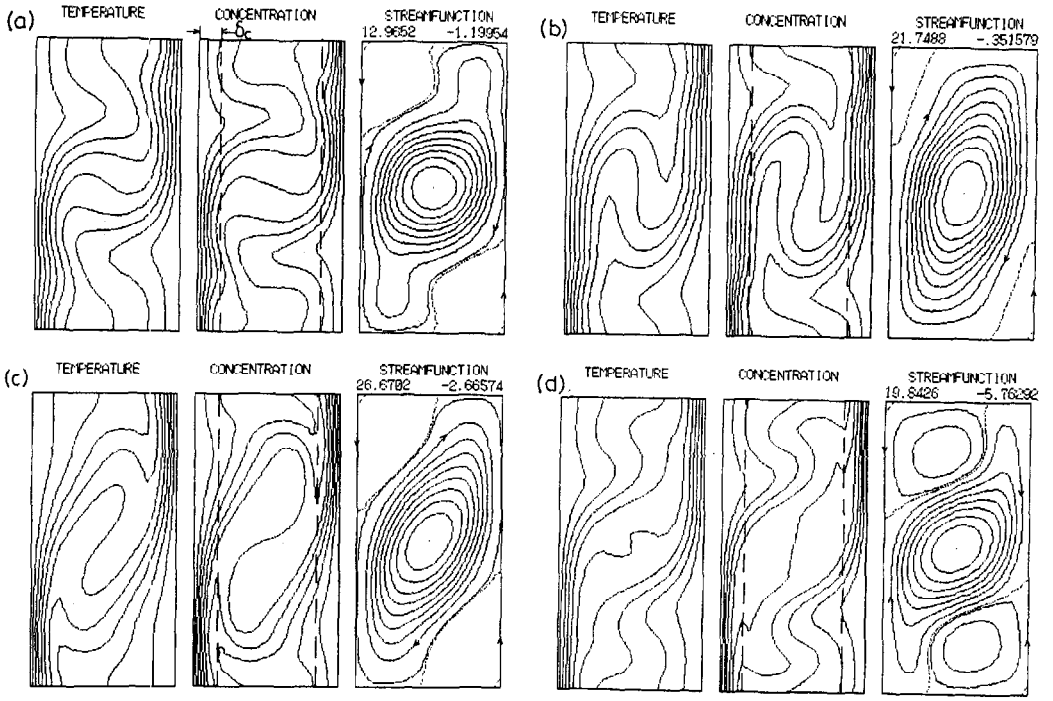

Fig. 5. Temperature, concentration and streamline contours during a period of oscillation at $N = 1.0$.

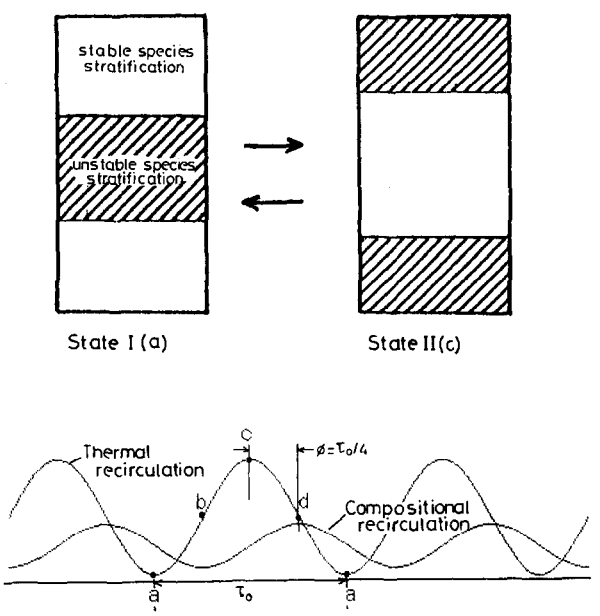

Fig. 6. Model of oscillation.

growth rate of thermal recirculation is reduced. During c–d, the unstable species stratification at the upper and lower parts is reduced, therefore the compositional recirculation is increased and the thermal recirculation is decreased. During d–a, the system makes ready for the following increase of thermal recirculation, and therefore the compositional recirculation is decreased and the decreasing rate of thermal recirculation is reduced. That is, the excitation process of thermal recirculation is during a–b, the inhibition process is during c–d, and the relaxation process is during b–c and d–a. If there is a 1/2 period delay between the thermal and the compositional recirculations, we cannot explain the periodic oscil-

lation using the three different processes because the relaxation process is not realized. Thus it is deduced that a periodic oscillation requires about 1/4 period delay between the thermal and compositional recirculations in the present system.

The reason for a periodic exchange between stable and unstable states in species stratification in the core region is due to the change in density near the vertical walls as a result of the thermosolutal instability as mentioned above. Figure 7 shows the density contours corresponding to Fig. 5. Higher density fluid is ejected from the hot wall at the location of 2/3 the enclosure height, and lower density fluid is ejected from the cold wall at the location of 1/3 the height, where there are stagnation points as shown in the streamlines of Fig. 5. The density stratification in the core changes periodically, which is significantly different from the density contours in thermal and compositional-dominated steady flows shown in Fig. 2. Higher and lower density fluids are generated from the compositional boundary layers along the vertical walls and this diffusion process has a high compositional resistance in the species transport processes, i.e., a limiting rate. Thus it appears that the period of oscillation due to the thermosolutal instability, t_0 is comparable to the time scale of species diffusing through the compositional boundary layer thickness, δ_c^2/D. As a result, the dimensionless period of oscillation τ_0 is represented by $(\delta_c^2/W^2)Le$, which is independent of buoyancy ratio as indicated by the numerical results. So, we estimate the boundary layer thickness δ_c from the dimensionless period of oscillation. The predicted value of δ_c is denoted by the dotted line in Fig. 5 and it satisfactorily corresponds to the dense zone of concentration contours.

Figure 8 shows time profiles of overall Nusselt and Sherwood numbers. The time variations are similar between them, but there is a small phase lag. The maxima in Nusselt and Sherwood numbers occur between the maximum thermal and compositional recirculation points shown in Fig. 4.

Bifurcation structure

The system under investigation bifurcates among steady and oscillatory states at some critical values of buoyancy ratio. Dual solutions exist due to highly nonlinear nature of the system to characterize the bifurcations, we analyzed the time profile in the two courses of changing buoyancy ratio, i.e., increasing and decreasing buoyancy ratio. The bifurcation diagram is shown in Fig. 9 as a function of buoyancy ratio. The ordinate denotes the strength of thermal and compositional recirculations. In the figure, the oscillatory state is indicated by pairs of open circles, which represent the maximum and minimum values of each recirculation during a period of oscillation, while the steady state is shown by a single closed circle. We focus on the behavior of thermal recirculation, because the result of compositional recirculation shows the same trend.

The bifurcation points are denoted by B1, B2 and B3. The system shifts from the steady thermal-dominated flow to the oscillatory flow at B1 ($N = 0.9$). This bifurcation gives no hysteresis, with the oscillation amplitude growing continuously from an infinitely small value. On the other hand, the bifurcation at B2 ($N = 1.044$) exhibits hysteresis (the hatched zone in the figure). That is, the system passes from the oscillatory flow to the steady compositional-dominated flow at B3 ($N = 1.122$) while it bifurcates from the compositional-dominated flow to the oscillatory flow at B2. The oscillation tends to start or terminate discontinuously. Comparison of thermal and compositional recirculations reveals that oscillatory flow occurs in the thermal-dominated flows. Figure 10 shows a bifurcation diagram of the overall Sherwood numbers for reference. The trend is the same as the result of Fig. 9. In the course of increasing buoyancy ratio, the Sherwood number decreases up to bifurcation point B3 and then increases. However, in the reverse course the Sherwood number decreases up to B2, and increases.

Thus oscillatory flows are classified into two regions with and without hysteresis, respectively. In the previous studies [21, 22] we discovered hysteresis for two different steady flows for $A = 0.5$ and 1 under the same flow conditions, and oscillatory and steady flows for $A = 2$, for a given buoyancy ratio.

The observed bifurcation structure of double-

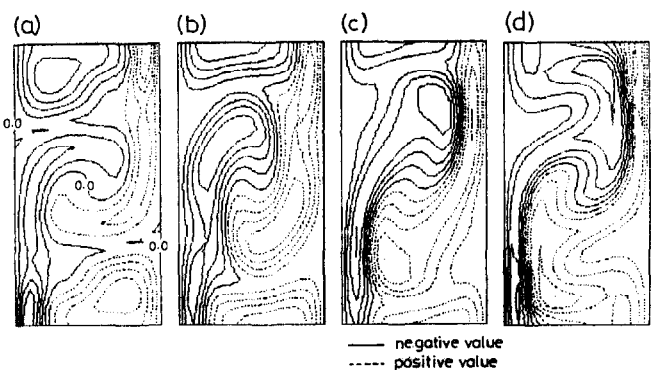

Fig. 7. Density contours during a period of oscillation at $N = 1.0$.

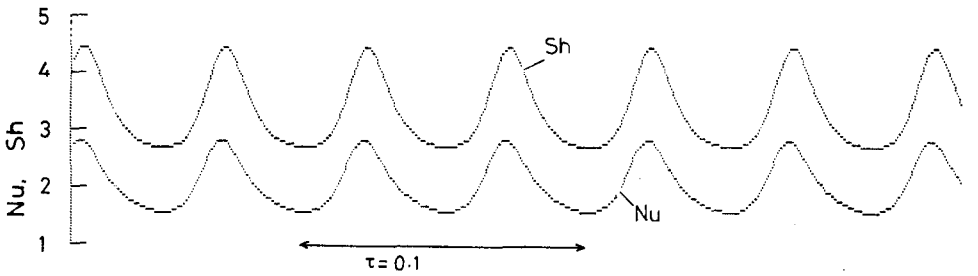

Fig. 8. Time profiles of Nusselt and Sherwood numbers at $N = 1.0$.

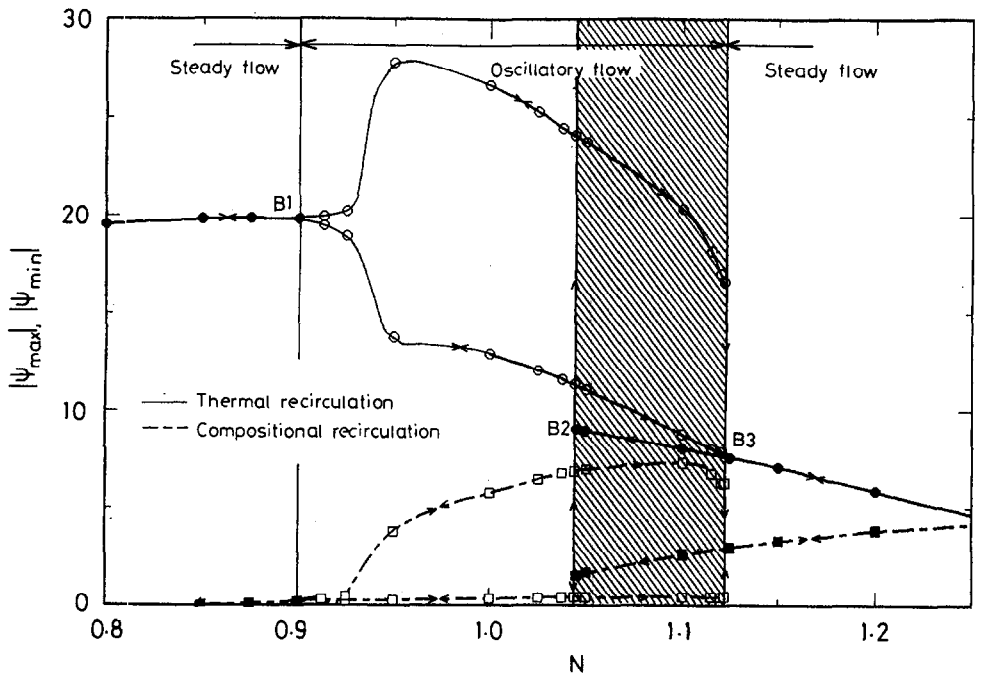

Fig. 9. Bifurcation diagrams of thermal and compositional recirculations.

diffusive convection has not been reported previously. However, a similar bifurcation was found experimentally for the chemical oscillation by Mori and Hanazaki [26] who examined the pH value of the reaction mixture in the $Fe(CN)_6^{4-}$–H_2O_2–H_2SO_4 system in a continuous flow stirred reactor. In this system, the pH value of the reaction mixture shows periodic oscillations in a certain range of residence time of reactants, e.g., flow rate. Although the present physical system is quite different from the chemical system, the qualitative mechanism of oscillation may be similar. This is the subject of future work.

CONCLUSIONS

We studied numerically oscillatory double-diffusive convection in a rectangular enclosure filled with binary gas, due to horizontal opposing temperature and concentration gradients imposed across the vertical walls. In particular, the effect of buoyancy ratio was considered under the conditions of $Ra_T = 10^5$, $Pr = 1$ and $Le = 2$. The following conclusive remarks have been drawn:

(1) Oscillatory flow occurs in a limited range of buoyancy ratio, i.e., $N = 0.9$ to 1.122, including the thermal-dominated flow regime with the secondary cell flow structure and is caused by a periodic exchange between stable and unstable states in species stratification, due to the interaction between thermal and compositional recirculations.
(2) The mechanism of oscillatory flow is believed to be the thermosolutal instability, and the periodic oscillation is explained by the three processes of excitation, relaxation and inhibition of the thermal recirculation. The period of oscillation is comparable to the time scale of the compositional boundary layer at the vertical wall.
(3) Hysteresis of steady and oscillatory states is ident-

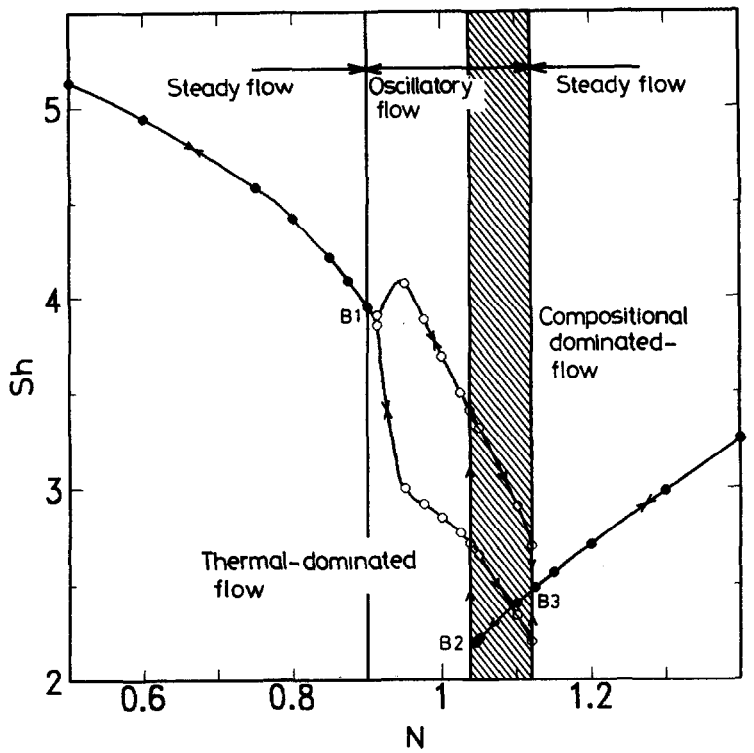

Fig. 10. Bifurcation diagram of Sherwood number.

ified in a certain range of buoyancy ratio, i.e., $N = 1.044$ to 1.122.

In the future, we explore the Lewis and Rayleigh number effects in this system.

REFERENCES

1. Rosenberger, F. and Muller, G., Interfacial transport in crystal growth, A parametric comparison of convective effects. *J. Crystal Growth*, 1983, **65**, 91–104.
2. Markham, B. I. and Rosenberger, F., Diffusive convective vapor transport across horizontal and inclined rectangular enclosures. *J. Crystal Growth*, 1984, **67**, 241–254.
3. Komiyama, H., Present status of research on chemical vapor deposition methods and significance of chemical engineering approach. *Kagaku Kogaku Ronbunshu*, 1990, **16**, 415–429.
4. Ostrach, S., Fluid dynamics in crystal growth—the 1982 Freeman scholar lecture, *ASME J. Fluid Eng.*, 1982, **105**, 5–20.
5. Beckermann, C. and Viskanta, R., Double diffusive convection during dendritic solidification of a binary mixture, *Phys. Chem. Hydrodyn.*, 1988, **10**, 195–213.
6. Christenson, M. S., Bennon, W. D. and Incropera, F. P., Solidification of an aqueous ammonium chloride solution in a rectangular cavity—II. Comparison of predicted and measured results. *Int. J. Heat Mass Transfer*, 1989, **32**, 69–79.
7. Nishimura, T., Fujiwara, M. and Miyashita, H., Double-diffusive convection during solidification of a binary system, *Heat Transfer Jpn. Res.*, 1992, **21**, 586–600.
8. Nishimura, T., Imoto, T. and Miyashita, H., Occurrence and development of double-diffusive convection during solidification of a binary system, *Int. J. Heat Mass Transfer*, 1994, **37**, 1455–1464.
9. Kamotani, Y., Wang, L. W., Ostrach, S. and Jiang, H. D., Experimental study of natural convection in shallow enclosures with horizontal temperature and concentration gradients, *Int. J. Heat Mass Transfer*, 1985, **28**, 165–173.
10. Jiang, H. D., Ostrach, S. and Kamotani, Y., Thermosolutal convection with opposed buoyancy forces in shallow enclosures, *ASME-HTD*, 1988, **99**, 53–66.
11. Chang, J. and Lin, T. F., Unsteady thermosolutal opposing Convection of liquid-water mixture in a square cavity—II. Flow structure and fluctuation analysis, *Int. J. Heat Mass Transfer*, 1993, **36**, 1333–1345.
12. Bergman, T. L. and Hyun, M. T., Simulation of two-dimensional thermosolutal convection in liquid metals induced by horizontal temperature and species gradients, *Int. J. Heat Mass Transfer*, 1996, **39**, 2883–2894.
13. Weaver, J. A. and Viskanta, R., Natural convection in binary gases due to horizontal thermal and solutal gradients, *ASME J. Heat Transfer*, 1991, **113**, 141–147.
14. Tsitverblit, N., Bifurcation phenomena in confined thermo-solutal convection with lateral heating: commencement of the double-diffusive region, *Phys. Fluids A*, 1995, **7**, 718–736.
15. Kamakura, K. and Ozoe, H., Oscillatory double diffusive natural convection in a two-layer system. *Proc. of 10th Int. Heat Transfer Conference*, 1994, **7**, 67–72.
16. Wee, H. K., Keey, R. B. and Cunningham, M. J., Heat and mass transfer by natural convection in a rectangular cavity, *Int. J. Heat Mass Transfer*, 1989, **32**, 1765–1778.
17. Beghein, C., Haghighat, F. and Allard, F., Numerical study of double-diffusive natural convection in a square cavity, *Int. J. Heat Mass Transfer*, 1992, **35**, 833–846.
18. Ranganthan, P. and Viskanta, R., Natural convection in a square cavity due to combined driving forces, *Numerical Heat Transfer*, 1988, **14**, 35–59.

19. Nishimura, T. and Kawamura, Y., Numerical errors of the Galerkin finite-element method for natural convection of a fluid layer or a fluid-saturated porous layer. *Numerical Heat Transfer A*, 1992, **22**, 241–255.
20. Nishimura, T., Nakagiri, H. and Kunitsugu, K., Flow patterns and wall shear stresses in grooved channels at intermediate Reynolds numbers: effect of groove length, *Trans JSME Ser. B*, 1996, **62**, 2106–2112.
21. Gobin, D. and Bennacer, R., Double diffusion in a vertical fluid layer: onset of the convective regime, *Phys. Fluids A*, 1994, **6**, 59–67.
22. Lee, J. W. and Hyun, J. M., Double-diffusive convection with opposing horizontal temperature and concentration gradients, *Int. J. Heat Mass Transfer*, 1990, **33**, 1619–1632.
23. Nishimura, T., Imoto, T. and Wakamatsu, M., A numerical study of the structure of double-diffusive natural convection in a square cavity, *Proc. of 4th ASME/JSME Thermal Eng. Conference*, 1995, **1**, 193–200.
24. Nishimura, T., Imoto, T. and Wakamatsu, M., A numerical study of double-diffusive natural convection in a rectangular enclosure filled with binary gas, *Trans JSME Ser. B*, 1996, **62**, 271–277.
25. Paolucci, S. and Chenoweth, D. R., Transition to chaos in a differentially heated vertical cavity, *J. Fluid Mech.*, 1989, **201**, 379–410.
26. Mori, Y. and Hanazaki, I., Bifurcation structure of the chemical oscillation in the $Fe(CN)_6^{4-}$–H_2O_2–H_2SO_4 system. *J. Phys. Chem.*, 1993, **97**, 7375–7378.
27. Morega, A. M. and Nishimura, T., Double-diffusive convection by a Chebyshev collocation method, Technology Reports of the Yamaguchi University, 1996, **5**, 259–276.

APPENDIX

We compared the present finite element solutions with spectral solutions to confirm the numerical accuracy. Spectral solutions are obtained by a Chebyshev collocation technique [27], whose advantage over finite difference and finite element methods is characterized by the rapid decay of approximation errors as the spectral resolution is increased.

For example, we show the case of an oscillatory flow for $N = 1$. In Fig. A1, spectral and finite element results are compared in terms of concentration contours at time moments (a) and (d) of Fig. 5 (thin line for spectral solution with 40×80 points and a notched line for finite element output with 31×41 points). The good agreement confirms the numerical accuracy of both methods. Table A1 compares some relevant results as produced by the two numerical schemes: period of oscillation; streamfunction extrema, $|\Psi_{max}|$ and $|\Psi_{min}|$, which indicate the strength of thermal and compositional recirculations. The agreement is satisfactory for all physical quantities, which confirms that the present finite element solutions for 31×41 nodal points provides accurate results.

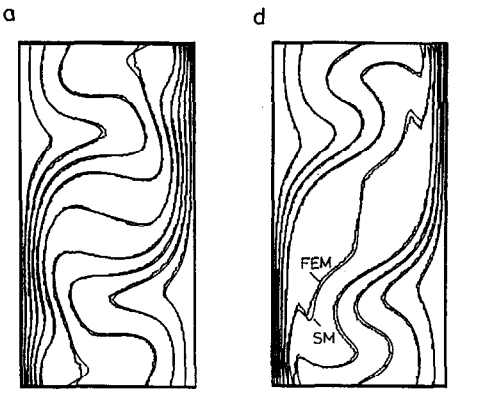

Fig. A1. Comparison between finite element method and spectral method for concentration contours.

Table A1. Comparison between the two numerical methods for $N = 1$

	Finite element method (31×41 points)	Spectral method (40×80 points)
τ_0	0.0497	0.0494
Max $\lvert\Psi_{max}\rvert$	26.7	26.8
Min $\lvert\Psi_{max}\rvert$	12.9	12.7
Max $\lvert\Psi_{min}\rvert$	5.76	5.52
Min $\lvert\Psi_{min}\rvert$	0.351	0.333